**CZECH TECHNICAL UNIVERSITY IN PRAGUE**

**Faculty Of Mechanical Engeneering**

Department of Technical Mathematics

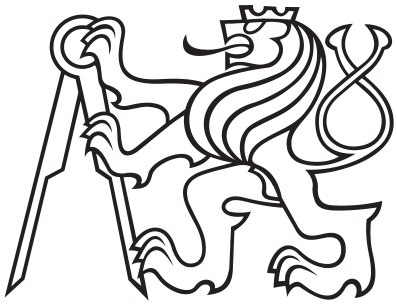

# SEMESTRAL PROJECT

Internal High-Speed Aerodynamics

# NUMERIACAL SIMULATIONS OF TWO-DIMENSIONAL, COMPRESSIBLE, INVISCID FLOWS WITH VARIOUS VALUES OF HEAT CAPACITY RATIO - $\gamma$

**Author:** Ing. Josef Musil

**Lecturer:** Prof. Ing. Pavel Šafařík, CSc.

**Consultant:** Doc. Ing. Jiří Fürst, Ph.D.

**Academic year:** 2018/2019

České vysoké učení technické v Praze
Fakulta strojní

# Zadání úkolu v předmětu

# Vnitřní aerodynamika při vysokých rychlostech

pro p. Ing. Josefa MUSILA

Název zadání :
**Numerická simulace proudění stlačitelné a nevazké tekutiny pro různé poměry měrných tepelných kapacit**

Úkol :

1. Připravte podklady pro numerickou simulaci proudění stlačitelné a nevazké tekutiny pro různé poměry měrných tepelných kapacit.
2. Formulujte úlohu a připravte program pro řešení parametrů proudu stlačitelné a nevazké tekutiny ve špičkové lopatkové mříži.
3. Proveďte numerickou simulaci a řešte proudění stlačitelné a nevazké tekutiny pro poměry měrných tepelných kapacit $\kappa$ = 1,4, 1,66, 1,33 a 2,0 ve špičkové lopatkové mříži.
4. Proveďte diskusi dosažených výsledků řešení a rozbor parametrů proudění stlačitelné a nevazké tekutiny pro různé poměry měrných tepelných kapacit.

Doporučená literatura :

1. A.H.Shapiro : *The Dynamics and Thermodynamics of Compressible Fluid Flow*, The Ronald Press Company, New York, 1954
2. J.Blazek : *Computational Fluid Dynamics : Principles and Applications*, Elsevier, Oxford, 2005
3. J.H.Ferziger, M.Perić : *Computational Methods for Fluid Dynamics*, Springer, Berlin, 2002
4. R.Dvořák, K.Kozel : Matematické modelování v aerodynamice, Vydavatelství ČVUT, Praha, 1996
5. další odborná a internetová literatura.

Rozsah :
15 stran textu včetně obrázků
15 minut přednáška

Lektor předmětu:
Prof.Ing.Pavel Šafařík,CSc.

Konzultant předmětu :
Doc.Ing.Jiří Fürst,PhD.

Praha 17. října 2018

# Contents



# Abbreviations

| | | |
|---|---|---|
| $\rho$ | density | $[kg/m^3]$ |
| $\vec{u}$ | velocity vector | $[m/s]$ |
| $u$ | velocity component in $x$-direction | $[m/s]$ |
| $v$ | velocity component in $y$-direction | $[m/s]$ |
| $\hat{u}$ | specific internal energy | $[J/kg]$ |
| $e$ | specific total energy | $[J/kg]$ |
| $h$ | specific enthalpy | $[J/kg]$ |
| $q$ | specific heat | $[J/kg]$ |
| $p$ | pressure | $[Pa]$ |
| $T$ | thermodynamic temperature | $[K]$ |
| $t$ | time | $[s]$ |
| $c_p$ | specific heat capacity at constant pressure | $[J/kg/K]$ |
| $c_v$ | specific heat capacity at constant volume | $[J/kg/K]$ |
| $f$ | number of degrees of freedom | $[-]$ |
| $r$ | specific gas constant | $[J/kg/K]$ |
| $k$ | Boltzmann constant | $[kg \cdot m^2/s^2/K]$ |
| $g$ | gravitational acceleration | $[m/s^2]$ |
| $\gamma$ | ratio of heat capacities | $[-]$ |
| $c$ | speed of sound | $[m/s]$ |
| $(\cdot)_\xi$ | partial derivative with respect to arbitrary variable | |
| $x, y, z$ | spatial coordinates | |
| $\alpha_{bl}$ | stagger angle of blade | $[°]$ |
| $\iota$ | incidence angle | $[°]$ |

# 1. Introduction

In classical thermodynamics, the physical quantities referred as heat capacities plays vital role in determination of thermal properties of given system. They essentially describe how heat delivered to the system is distributed between energy related with thermodynamic temperature and other forms of energy, typically expressed by internal energy. The whole process of heat transfer in/out of the system is usually studied with restrictive condition, stating that one chosen parameter of the system is being fixed. The following terms express perhaps the most commonly used heat capacities.

$$\left(\frac{\partial \hat{u}}{\partial T}\right)_v = \left(\frac{\partial q}{\partial T}\right)_v = c_v, \qquad \left(\frac{\partial h}{\partial T}\right)_p = \left(\frac{\partial q}{\partial T}\right)_p = c_p \tag{1.1}$$

With $c_v$ resp. $c_p$ being specific heat capacities at constant volume resp. pressure. Note, that the equations 1.1 are independent of the type of thermodynamic process or substance going through the process.

According to the statistical thermodynamics, the equipartition theorem states, that in equilibrium, each degree of freedom contributes $\frac{1}{2}kT$ to the average energy per molecule. Thus by simple calculation one gets relation for specific internal energy, and subsequently, specific heat capacity at constant volume

$$\hat{u} = \frac{1}{2} frT \qquad c_v = \left(\frac{\partial \hat{u}}{\partial T}\right)_v = \frac{f}{2} r \tag{1.2}$$

where $f$ denotes number of degrees of freedom of one molecule, $r$ is specific gas constant.

Considering further only systems of gaseous phase described by equation of state of ideal gas, the various values of heat capacity ratio - $\gamma$, could be expressed, with using Mayer's relation, in the following way

$$\gamma = \frac{c_p}{c_v} = \frac{c_v + r}{c_v} = \frac{fr/2 + r}{fr/2} = 1 + \frac{2}{f}. \tag{1.3}$$

Now, equipped with this information, one can view the study of flows with varied $\gamma$ as a series of cases where gases with different degrees of freedom were used. With respect to the objectives of this work, following table summarizes given values of $\gamma$ and link them with the physical interpretation.

**Table 1.1:** Variation of heat capacity ratio

| $\gamma$ | degrees of freedom - $f$ | physical interpretation |
|---|---|---|
| 1.33 | 6 | three and more atoms in molecule **without** the vibrational degrees of freedom (not considering straight molecules) |
| 1.40 | 5 | diatomic gas molecule **without** the vibrational degree of freedom |
| 1.66 | 3 | monoatomic gas |
| 2.00 | (2) | "monoatomic gas in 2 dimmensions" or shallow water analogy (Subsection 1.1) |

## 1.1 Analogy of shallow water equations with Euler equations for $\gamma = 2$

The physical meaning of first three values of $\gamma$ in table 1.1 is rather clear. The most commonly used value, $\gamma = 1.4$, sufficiently describes air in quite wide range of thermodynamical states, and it is also considered as a standard value. If diatomic gas is considered in higher temperatures, vibration of each atom in the molecule becomes large enough to store some of the heat energy supplied to the system so one additional degree of freedom is added, resulting in $\gamma = 1.33$. The monoatomic gas ($\gamma = 1.66$) is not used in experimental studies for number of obvious reasons.

If we take a look on $\gamma = 2$ then no reasonable interpretation in terms of thermodynamical properties can be assigned to this value. However, there is a useful similarity between Euler equations of fluid motion and shallow water equations. This analogy can be used while designing some experiments dealing with fluid flow around the objects. Especially in the case of transsonic regimes of the flow around the turbine blades.

Consider the one-dimensional Euler equations for adiabatic flows written in terms of $\rho$ and $u$ in matrix form

$$\begin{pmatrix} \rho \\ u \end{pmatrix}_t + \begin{pmatrix} u & \rho \\ \frac{c^2}{\rho} & u \end{pmatrix} \begin{pmatrix} \rho \\ u \end{pmatrix}_x = \begin{pmatrix} 0 \\ 0 \end{pmatrix} \tag{1.4}$$

where $c = \sqrt{C\gamma\rho^{\gamma-1}}$ denotes speed of sound in ideal gas with constant $\gamma$ and $C \in \mathbb{R}$ is constant depending on the specific internal energy of the system. These equations can be also re-arranged using the theory of characteristics. In a new form there are employed new variables called Riemann invariants, depending on the original variables

$$\frac{\partial J_+}{\partial t} + (u + c)\frac{\partial J_+}{\partial x} = 0, \qquad \frac{\partial J_-}{\partial t} + (u - c)\frac{\partial J_-}{\partial x} = 0 \tag{1.5}$$

where $J_\pm = u \pm \frac{2}{\gamma-1}c$ are Riemann invariants. On the other hand, one can obtain exactly one-dimensional shallow water equations in invariant form by setting $\gamma = 2$ and $C = \frac{g}{2}$ and substituting density $\rho = \rho(x)$ for water height $h = h(x)$.

# 2. Mathematical model of compressible inviscid flow

The fluids studied in this work are considered to be compressible and inviscid and therefore can be described by Euler equations for ideal gas.

**Continuity equation**

$$\frac{\partial \rho}{\partial t} + \nabla \cdot (\rho \mathbf{u}) = 0 \tag{2.1}$$

**Momentum equation**

$$\frac{\partial (\rho \mathbf{u})}{\partial t} + \nabla \cdot (\rho \mathbf{u} \otimes \mathbf{u}) + \nabla p = 0 \tag{2.2}$$

**Energy equation**

$$\frac{\partial (\rho e)}{\partial t} + \nabla \cdot \Big( (e+p)\rho \mathbf{u} + \Big) = 0 \tag{2.3}$$

The system (2.1 - 2.3) is closed by the equation of state for ideal gas:

$$p = (\gamma - 1)\left(\rho e - \frac{1}{2}\rho |\mathbf{u}|^2\right) \tag{2.4}$$

There will be further considered only two-dimensional flows through the tip-section of the last stage of steam turbine. Therefore the vector quantities in the above equations (2.1-2.4) will consist only of two components, in $x$ and $y$ directions. Particularly, the velocity will has form of $\mathbf{u} = (u, v)$. With respect to further proceeding the Euler equations can be also expressed in more compact form

$$\frac{\partial \mathbf{W}}{\partial t} + \mathsf{div}_{\mathbf{x}} \left( \mathbb{F}(\mathbf{W}) \right) = \mathbf{0} \tag{2.5}$$

where $\mathbf{W} = [\rho, \rho\mathbf{u}, \rho e]$ is the vector of conservative variables and its fluxes is represented by $\mathbb{F}(\mathbf{W}) = [\rho\mathbf{u}, \rho\mathbf{u} \otimes \mathbf{u} + p\mathbb{I}, (e+p)\rho\mathbf{u}]$. Therefore Euler equations are inviscid, no additional models of turbulence are needed to close them, so now, the discretization procedure by finite volume method will follow.

# 3. Numerical solution

## 3.1 Finite volume method

Firstly, let us integrate Euler equations (2.5) over the fixed spatial domain

$$\int_{\Omega} \frac{\partial \mathbf{W}}{\partial t}\, dV + \int_{\Omega} \mathsf{div}_{\mathbf{x}} \left(\mathbb{F}(\mathbf{W})\right)\, dV = \mathbf{0} \tag{3.1}$$

where $\Omega \subset \mathbb{R}^2$ is whole domain where equations (2.5) tend to solved and $\partial\Omega$ will denote domains boundary (expected to be Lipschitz continuous). Now, with respect to $\Omega$ being time independent and by using Gauss-Green formula, above equation can be written as

$$\frac{d}{dt} \int_{\Omega} \mathbf{W}(\mathbf{x}, t)\, dV + \int_{\partial\Omega} \mathbb{F}(\mathbf{W}(\mathbf{x}, t))\, dS = \mathbf{0} \tag{3.2}$$

Since the above integral identity holds for any non-zero arbitrary control domain $\Omega_i$ it could be now rewritten to the following form of the system of ordinary differential equations

$$|\Omega_i| \frac{d\mathbf{W}_i(t)}{dt} = -\sum_{j \in N_i} \mathbb{F}_{ij} \cdot \mathbf{S}_{ij} \tag{3.3}$$

where $\Omega_i \in \Omega = \bigcup \Omega_i$ and $\bigcap \Omega_i = \emptyset$, thus $\Omega_i$ represents arbitrary finite volume cell, assumed to be of polygonal, resp. polyhedral shape (in two, resp. three dimensions), see Fig. 3.1. Consequently, the boundary $\partial\Omega_i$ of $\Omega_i$ consists of union of connected lines, resp. polygonal faces. Furthermore, vector of conservative variables discretized in space using finite volume method $\mathbf{W}_i(t)$ is expressed as

$$\mathbf{W}_i(t) = \frac{1}{|\Omega_i|} \int_{\Omega_i} \mathbf{W}(\mathbf{x}, t)\, dV. \tag{3.4}$$

Finally, $N_i$ denotes set of indices of finite volume cells neighboring with $\Omega_i$ and $\mathbf{S}_{ij}$ is normal vector of face between cells $i$ and $j$ pointing to the cell $j$, with length equal to the area of the face. Note that in the equation (3.3) have not been introduced any approximation yet. The cell average value $\mathbf{W}_i(t)$ approximates values of $\mathbf{W}(\mathbf{x}, t)$ in the cell with second order of accuracy (for $\mathbf{W}(\mathbf{x}, t)$ being smooth in $\Omega_i$)

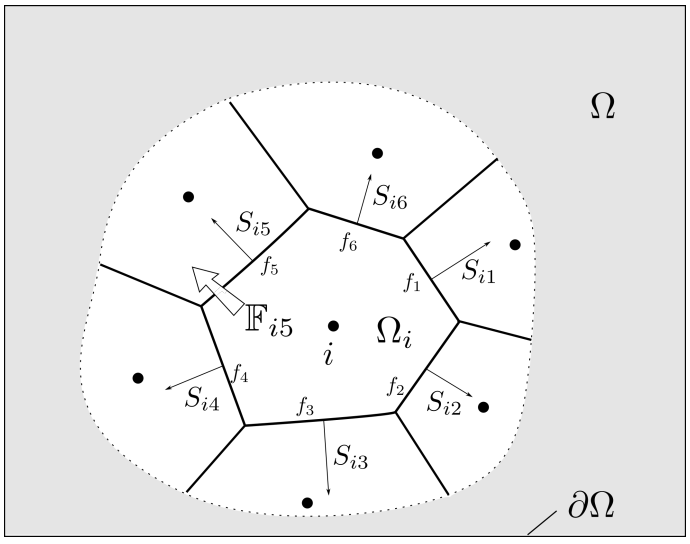


**Figure 3.1:** Schematic illustration of FVM.

## 3.2 Approximation of fluxes

Before writing down the equations (3.3) for all computational cells as a set of linear algebraic equations one has to do one final step - approximate the fluxes $\mathbb{F}_{ij}$. Several methods were developed for this purpose, however in this work is used so called HLLC scheme [1].

The HLLC scheme is a member of the family of so called Godunov's schemes which are conservative numerical schemes for solving partial differential equations based on solving exact or approximate Riemann problems at each inter-cell boundary. These were firstly introduced by S.K.Godunov [2]. Moreover the HLLC scheme build on top of the HLL scheme, presented by Harten, Lax and van Leer in [3].

The central idea of the HLL scheme is to solve Riemann problem at each cell rather approximately than exactly in order to save some computational expenses. This is done by neglecting intermediate (contact) wave, see Fig. 3.2. This approach has proven to be both efficient and robust, but in certain two and three-dimensional problems poor resolution of contact wave leads to unacceptable smearing of vortex sheets and shear waves [4]. In the case of HLLC scheme, the middle wave is restored using techniques similar to the ones used in derivation of HLL scheme. Furthermore, the whole reconstruction of intermediate wave involves several steps which are briefly described as follows:

A) Compute pressure estimate $p^*$ from known variables, $u_i, \rho_i, p_i$, $i = L, R$

B) Compute estimate of $S_L$ resp. $S_R$, speed of left resp. right wave from variables $u_i, \rho_i, p_i, p^*$, $i = L, R$

C) Compute HLLC flux from previous variables.

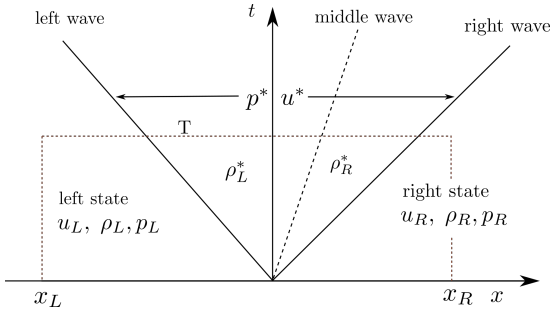


**Figure 3.2:** Solution of the Riemann problem with data $U_L$ and $U_L$ in the $x, t$-plane. The three waves present define four piece-wise constant states. Reconstructed figure from [4].

Note that there are several choices how to compute variables during steps I) - III), all of them are based on integration of equation (3.2) in the rectangle $[x_L, x_R] \times [0, T]$ in $x, t$-plane followed by linear approximation of intermediate states. Complete description of HLLC scheme is provided in i.e. [1].

## 3.3 Matrix-free LU-SGS numerical solver

Numerical solution of the system of non-linear ordinary differential equations (3.3) will be carried out by matrix-free lower-upper symmetric Gauss–Seidel (LU-SGS) numerical solver, implemented into OpenFOAM [5] by J.Fürst, see [6]. Short description of the implemented solver adopted form the original article follows.

The numerical simulations further studied in this work are considered to have steady state which will be the aim to reach in the computations. In order to do so, one can rewrite equations (3.3) as follows

$$|\Omega_i| \frac{\mathbf{W}_i^{n+1} - \mathbf{W}_i^n}{\Delta t_i} = -\sum_{j \in N_i} (\mathbb{F}_{ij} \cdot \mathbf{S}_{ij})^{n+1} = -\mathbf{R}(\mathbf{W}^{n+1})_i \tag{3.5}$$

where the time derivative has now meaning of pseudo-time marching and was replaced backward difference using local value of time step, $\Delta t_i$, and $\mathbf{R}(\mathbf{W^{n+1}})_i$ denotes residual

in $n+1$ iteration. The residual can be replaced by linear approximation

$$-\mathbf{R}(\mathbf{W}^{n+1})_i \approx -\mathbf{R}(\mathbf{W}^n)_i - \sum_j \frac{\partial \mathbf{R}(\mathbf{W}^n)_i}{\partial \mathbf{W}_j} \left(\mathbf{W}_j^{n+1} - \mathbf{W}_j^n\right) \tag{3.6}$$

leading to the following equation

$$\sum_j \left(\frac{|\Omega_i|}{\Delta t_i}\mathbb{I} + \frac{\partial \mathbf{R}(\mathbf{W}^n)_i}{\partial \mathbf{W}_j}\right) \left(\mathbf{W}_j^{n+1} - \mathbf{W}_j^n\right) = -\mathbf{R}(\mathbf{W}^n)_i \tag{3.7}$$

Here, in order to construct matrix-free solver, the Jacobian matrix $\partial \mathbf{R}(\mathbf{W}^n)_i / \partial \mathbf{W}_j$ is replaced by first order approximation of convective terms with Rusanov flux. Final form of low order residual replacement for inviscid flows reads

$$\mathbf{R}(\mathbf{W})_i^{lo} = \frac{1}{2}\sum_{j\in N_i} \lambda_{ij}\mathbf{W}_i + \frac{1}{2}\sum_{j\in N_i} (\mathbb{F}(\mathbf{W}_j)\cdot \mathbf{S}_{ij} - \lambda_{ij}\mathbf{W}_j) \tag{3.8}$$

where $\lambda_{ij}$ is the spectral radius of Jacobian of $\mathbb{F}\cdot\mathbf{S}$, i.e. $\lambda_{ij} = |\mathbf{u}_{ij}\cdot\mathbf{S}_{ij}| + a_{ij}|\mathbf{S}_{ij}|$ with $\mathbf{u}_{ij}$ being the velocity at the face between the cells $i$ and $j$ and $\mathbf{a}_{ij}$ is the sound speed.

Now rewriting LU-SGS algorithm for inviscid flow from original article one gets

$$D_i \Delta \mathbf{W}_i^{(1)} = -\mathbf{R}(\mathbf{W}^n)_i - \frac{1}{2}\sum_{j\in L_i} \left(\Delta \mathbb{F}_j^{(1)}\cdot \mathbf{S}_{ij} - \lambda_{ij}\Delta \mathbf{W}_j^{(1)}\right) \tag{3.9}$$

and

$$D_i \Delta \mathbf{W}_i = D_i \Delta \mathbf{W}_i^{(1)} - \frac{1}{2}\sum_{j\in U_i} (\Delta \mathbb{F}_j \cdot \mathbf{S}_{ij} - \lambda_{ij}\Delta \mathbf{W}_j) \tag{3.10}$$

where

$$D_i = \frac{|\Omega_i|}{\Delta t_i} + \frac{1}{2}\sum_{j\in N_i}\lambda_{ij}, \qquad \Delta \mathbf{W}_i^{(1)} = \mathbf{W}_i^{(1)} - \mathbf{W}_i^n, \qquad \Delta \mathbf{W}_i = \mathbf{W}_i^{n+1} - \mathbf{W}_i^n,$$
$$\Delta \mathbb{F}_i^{(1)} = \mathbb{F}(\mathbf{W}_i^{(1)}) - \mathbb{F}(\mathbf{W}_i^n), \quad \Delta \mathbb{F}_i = \mathbb{F}(\mathbf{W}_i^{n+1}) - \mathbb{F}(\mathbf{W}_i^n)$$

The summation indices $L_i = \{j \in N_i : j < i\}$ resp. $U_i = \{j \in N_i : j > i\}$ here denote sets of cells belonging to lower resp. upper of the system matrix. All the fluxes $\mathbb{F}(\mathbf{W}_i)$ are computed by previously described HLLC scheme.

# 4. Results

In this part there will be discussed results of numerical simulations of two-dimensional compressible flow through the tip-section linear blade cascade TR-U-6. The geometry and configuration of the cascade is depicted on Fig. 4.2. The computational mesh consists of approximately 82 000 cells of triangular shape which tend to grow in size towards the inlet and outlet boundary in order to dissipate possible shock-waves interacting with those boundaries, see Fig. 4.3. The mesh was created in open-source meshing software Gmsh.

The blade profile is designed with reversed curvature of suction side and the cascade is of convergent-divergent form causing low change of flow direction. The blade chord $c = 0.15$ m is given by the length measured along the linear part of the lower side of the blade profile. The parameter $s \approx 0.1514$ m denotes spacing between blades. The cascade is in constant position during the simulations with stagger angle $\alpha_{bl} = 79.28°$. Further information about cascade geometric parameters and configuration can be found in [7] or [8].

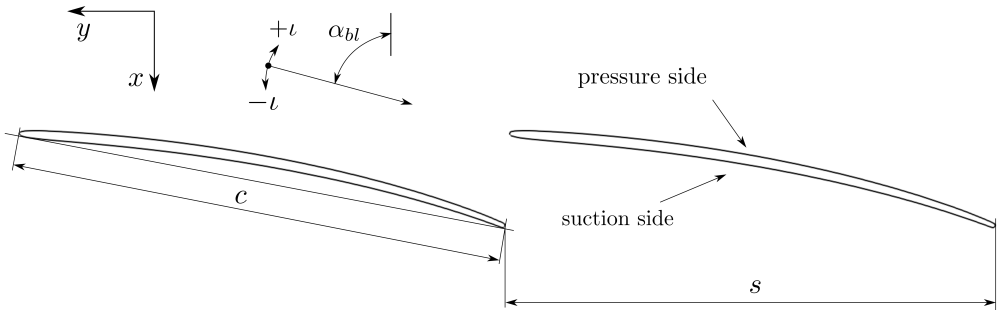


**Figure 4.1:** Scheme of linear blade cascade TR-U-6, adopted from [8].

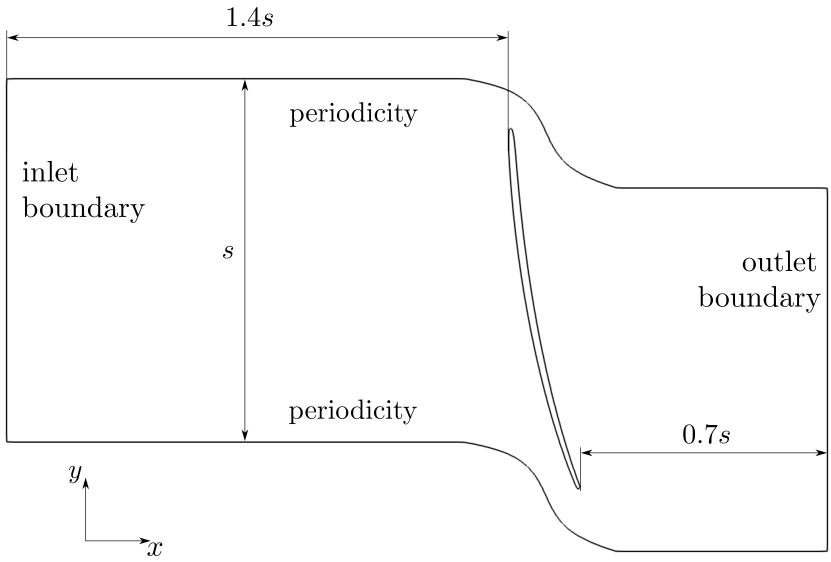


**Figure 4.2:** Scheme of computational domain.

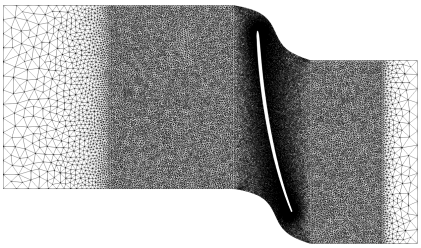

**Figure 4.3:** Computational mesh.

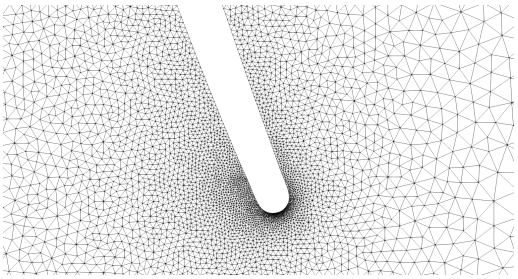

**Figure 4.4:** Detail of computational mesh.

The initial conditions were set as $p = 65 \times 10^3$ Pa, $\mathbf{u} = [20, -110]$ m/s, $T = 292$ K in whole computational domain for all the simulations. The boundary conditions were prescribed according to the table (4.1) and are prescribed in all the cases of varying heat capacity ratio. Thus $\gamma$ is the only varying parameter being studied in numerical simulations.

**Table 4.1:** Boundary conditions

| | $\mathbf{u}$ | $p$ | $T$ |
|---|---|---|---|
| **inlet** | specified direction of $\alpha_I = 79.78°$, $\lvert\mathbf{u}\rvert$ is calculated from Riemann invariant going along the outward directed characteristics | calculated from given stagnation pressure, $p_0 = 90 \times 10^3$ Pa using formulas [1] for insentropic compressible flow | calculated from total temperature, $T_0 = 292$ K using formulas [1] for insentropic compressible flow |
| **outlet** | homogeneous Neumann condition | fixed mean pressure, $p_{mean} = 40 \times 10^3$ Pa | homogeneous Neumann condition |
| **blade** | slip | homogeneous Neumann condition | homogeneous Neumann condition |

1)

$$\frac{p_0}{p} = \left(1 + \frac{\gamma - 1}{2} Ma^2\right)^{\frac{\gamma}{\gamma - 1}}, \quad \frac{T_0}{T} = 1 + \frac{\gamma - 1}{2} Ma^2, \quad Ma^2 = \frac{|\mathbf{u}|^2}{\rho r T}, \quad T = \frac{\gamma - 1}{r}\left(e - \frac{1}{2}|\mathbf{u}|^2\right)$$

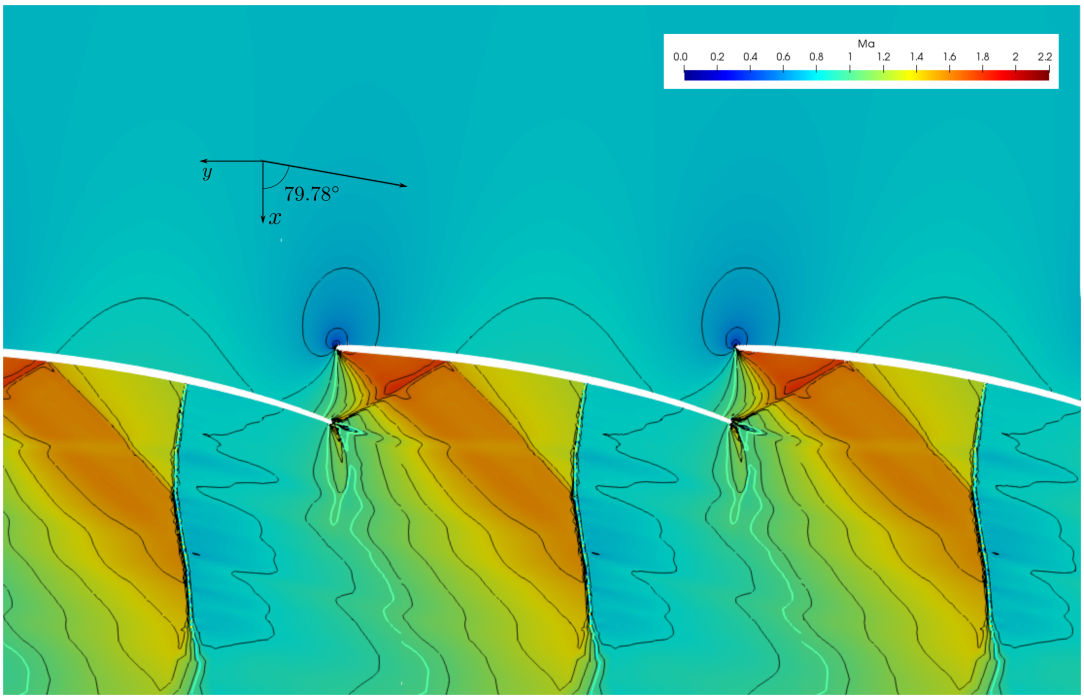


**Figure 4.5:** Mach number isolines, bold contour for $Ma = 1$, $\gamma = 1.33$.

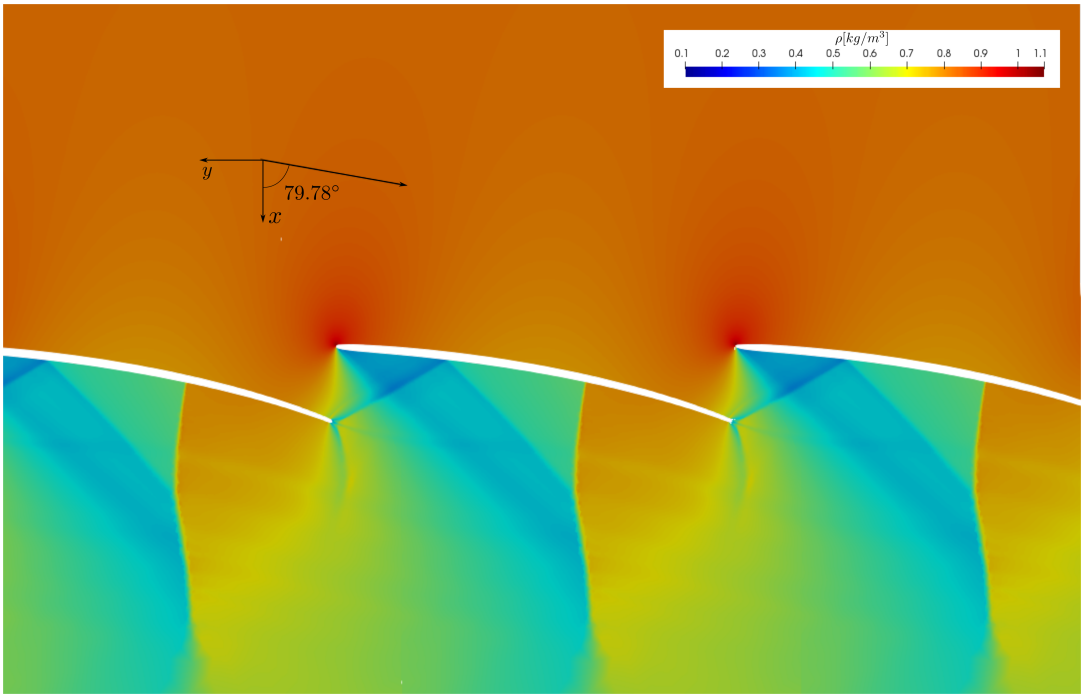


**Figure 4.6:** Density field, $\gamma = 1.33$.

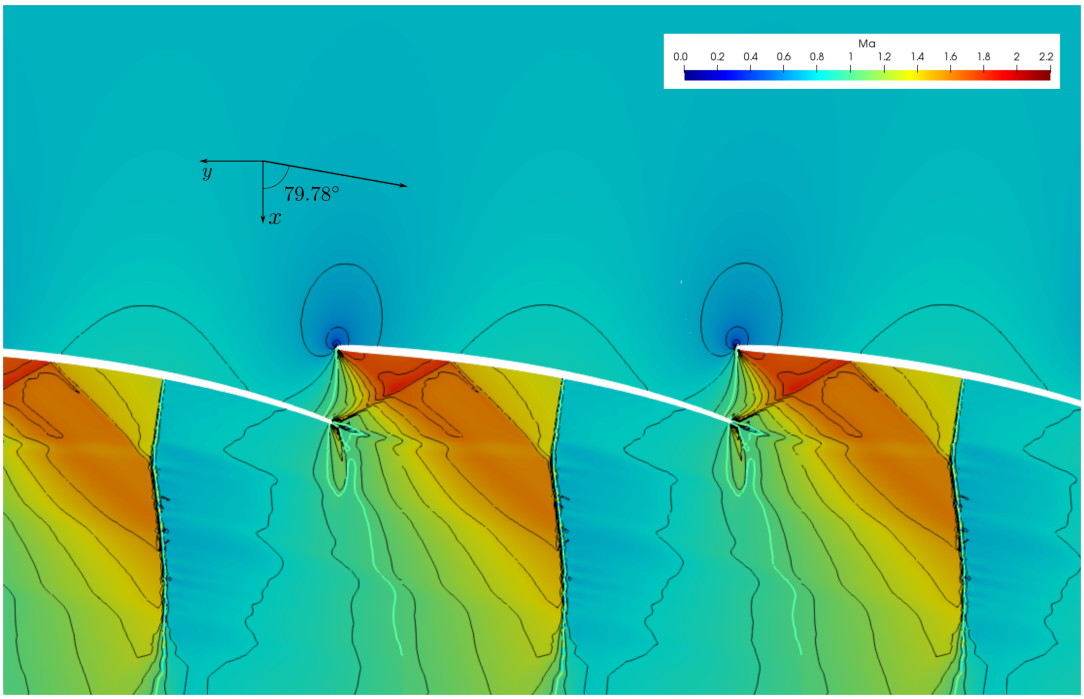


**Figure 4.7:** Mach number isolines, bold contour for $Ma = 1$, $\gamma = 1.4$.

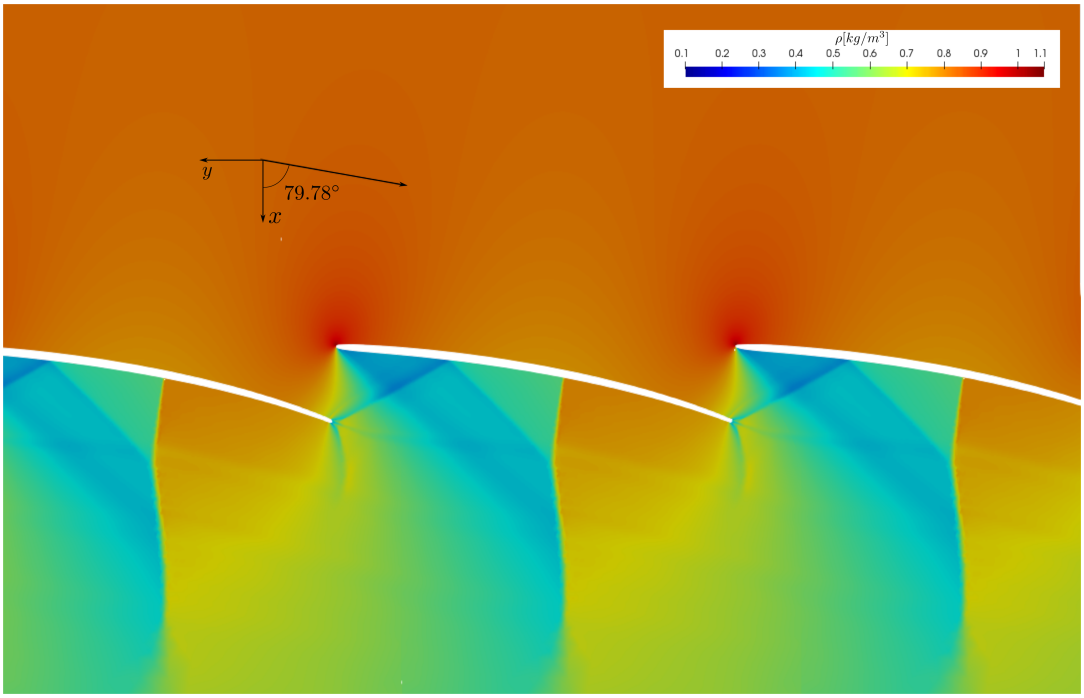


**Figure 4.8:** Density field, $\gamma = 1.4$.

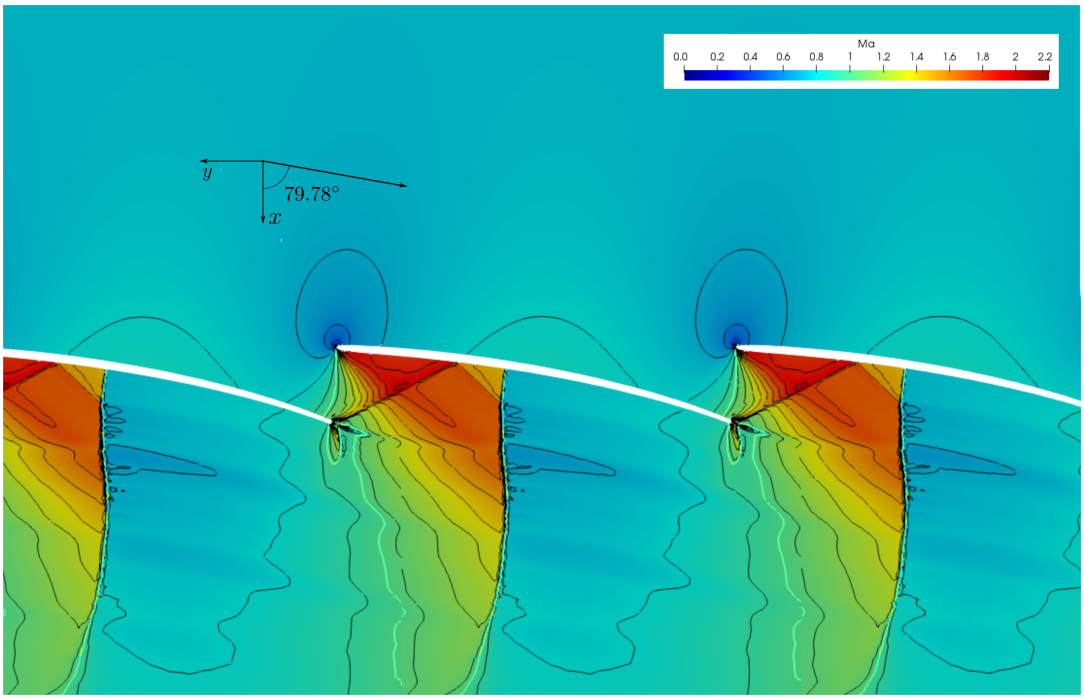


**Figure 4.9:** Mach number isolines, bold contour for $Ma = 1$, $\gamma = 1.66$.

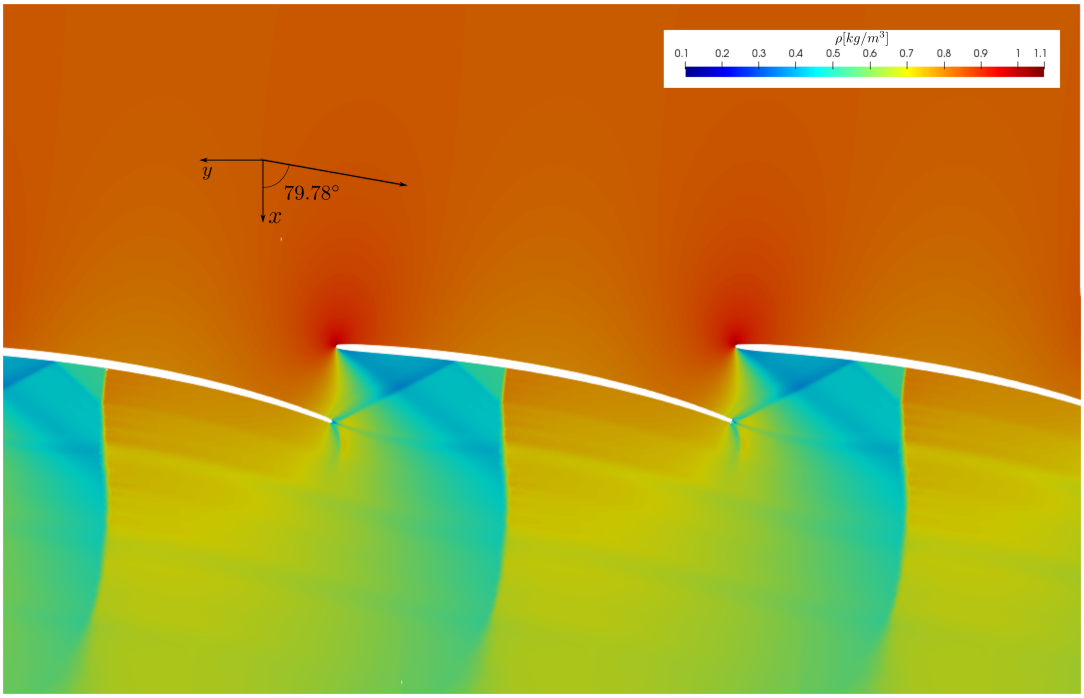


**Figure 4.10:** Density field, $\gamma = 1.66$.

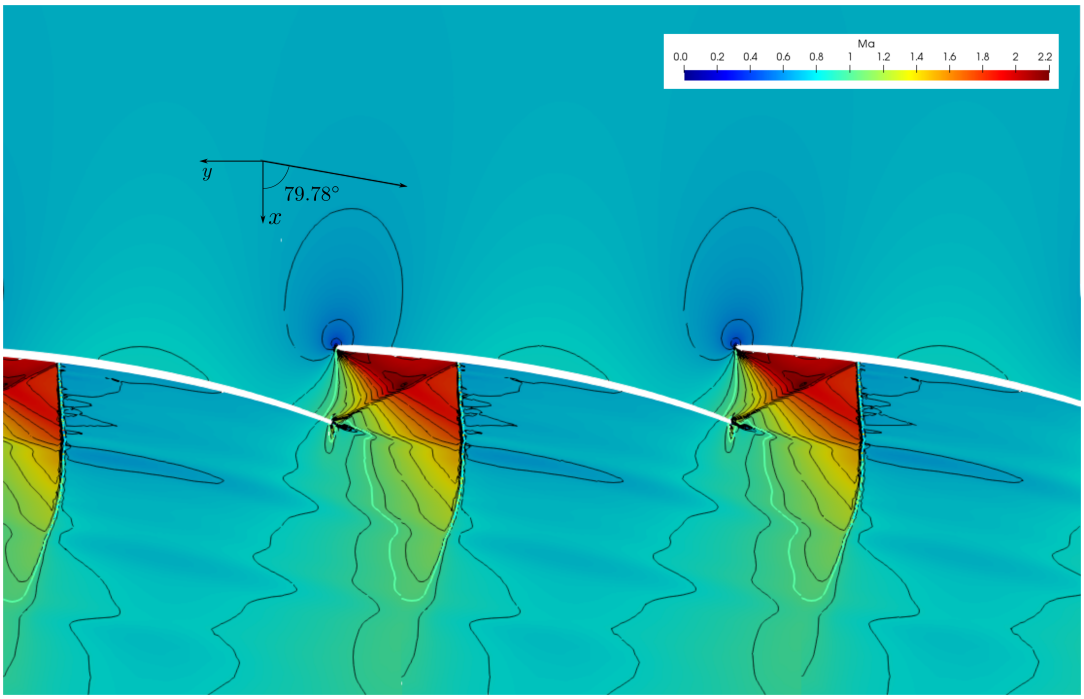


**Figure 4.11:** Mach number isolines, bold contour for $Ma = 1$, $\gamma = 2.0$.

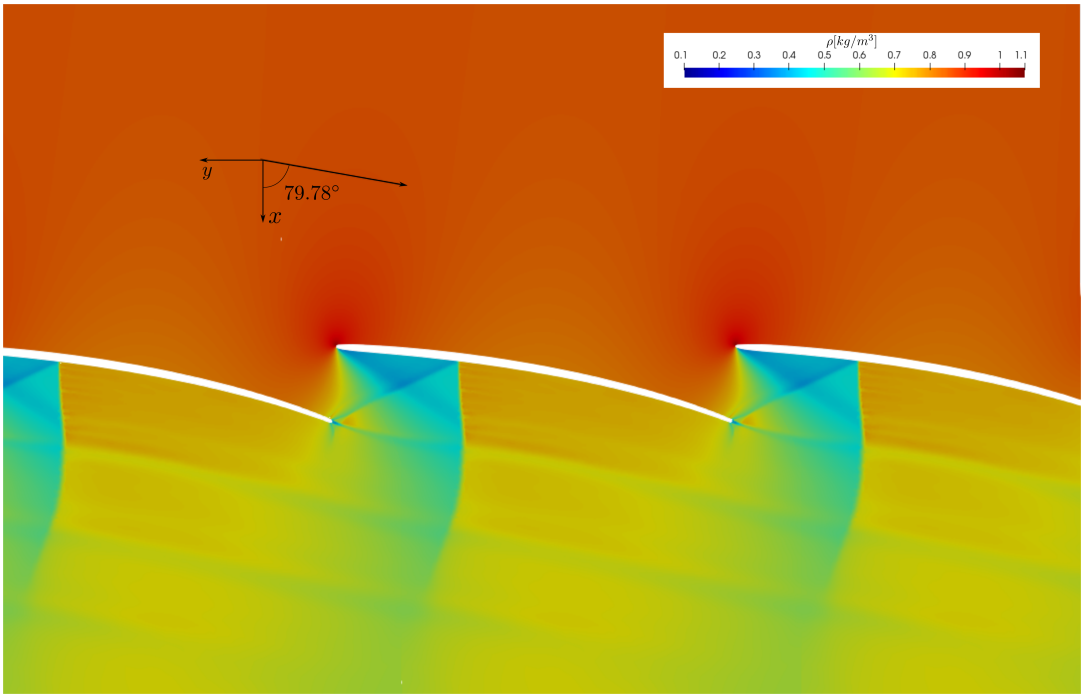


**Figure 4.12:** Density field, $\gamma = 2.0$.

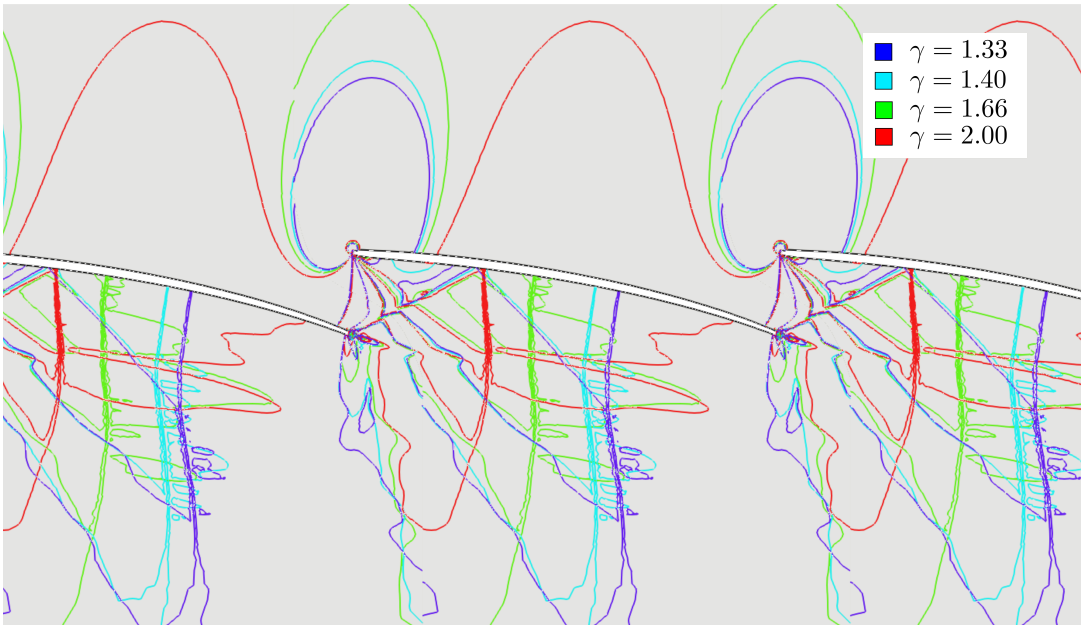


**Figure 4.13:** Contours of Mach number for $\gamma = 1.33, 1.4, 1.66, 2$.

# 5. Conclusion

On the above series of Figs. 4.5 - 4.13 there are displayed fields of Mach numbers and densities for various values of $\gamma$ in the blade cascade. There is depicted inlet flow angle $\alpha_I = 79.78°$ which corresponds, due to the geometrical configuration of the blade cascade, to the incidence angle $\iota = -0.5°$. One can observe small fluctuations downstream of the normal shock-wave in both Mach number and density fields. The reason of this behavior can be possibly explained by insufficient performance (instability) of HLLC flux scheme in this (inviscid) case leading to small unsteady changes in the flow when large gradients are present. There can be also seen slight effect of numerical viscosity in the vicinity of the trailing edge.

The main focus of the numerical experiments was variation of $\gamma$. This was proceeded under constant pressure difference between inlet and outlet, therefore isentropic Mach number, $Ma_{is}$, changed its values in the flow field causing the changes in position of normal shock-waves, see Fig. 4.13. Subsequently, regarding to this fact, the character of flow fields upstream of the normal shock-wave of $\gamma = 2$ is quite similar but the intensity of the fields is varying due to the faster resp. slower expansion being a consequence of higher resp. lower value of $\gamma$.

As mentioned in Section 1, the analogy of shallow water equations with Euler equations for adiabatic flows offers handful and relatively cheap method in experimental studies during the design process of turbine blades. This analogy is archieved by adjusting the corresponding parameters of these equations. However in last few decades the performance of computers along with numerical codes has improved offering even cheaper, faster and more precise option for turbine blades designing.

# References


[1] E. F. Toro. Riemann Solvers and Numerical Methods for Fluid Dynamics: A Practical Introduction. 2013.

[2] S. K. Godunov. A difference method for numerical calculation of discontinuous solutions of the equations of hydrodynamics. *Matematicheskii Sbornik*, 89(3):271–306, 1959.

[3] A. Harten, P. D. Lax, and B. van Leer. On Upstream Differencing and Godunov-Type Schemes for Hyperbolic Conservation Laws. *SIAM Rev*, 25:35–61, 01 1983.

[4] E. F. Toro, M. Spruce, and W. Speares. Restoration of the Contact Surface in the HLL-Riemann Solver. *Shock Waves*, 4:25–34, 07 1994.

[5] H. G. Weller, G. Tabor, H. Jasak, and C. Fureby. A Tensorial Approach to Computational Continuum Mechanics Using Object-oriented Techniques. *Comput. Phys.*, 12(6):620–631, November 1998.

[6] J. Fürst. Development of a coupled matrix-free lu-sgs solver for turbulent compressible flows. *Computers and Fluids*, 172:332 – 339, 2018.

[7] M. Luxa and D. Šimurda. Optická měření na mříži TR-U-6. Výzkumná zpráva. *ÚT AVČR, v.v.i. č., Praha*, 2014.

[8] P. Straka, J. Příhoda, and M. Bobčík. Simulation of Compressible Flow Through the Tip-Section Turbine Blade Cascade with the Unsteady Interaction of the Shock Wave with Shear Layers. 01 2016.